Spiral nuclear momentum distribution for the dissociation of H_2^+ in a circularly polarized laser pulse

Zhen Chen,[1] Pei-Lun He,[1] and Feng He[1,2,*]

[1]*Key Laboratory for Laser Plasmas (Ministry of Education) and Department of Physics and Astronomy, Collaborative Innovation Center of IFSA (CICIFSA), Shanghai Jiao Tong University, Shanghai 200240, China*

[2]*CAS Center for Excellence in Ultra-intense Laser Science, Shanghai 201800, China*

(Received 16 July 2019; accepted 19 February 2020; published 11 March 2020)

The dissociation of H_2^+ in a circularly polarized laser pulse is numerically studied by simulating the time-dependent Schrödinger equation. After absorbing one or three photons, the nuclear wave packets carrying the angular momenta $\hbar$ and $3\hbar$ dissociate along the $2p\sigma_u$ state. Due to the broad initial kinetic-energy distribution of the superimposed nuclear vibrational states, the one-photon and three-photon dissociation pathways may end with the same kinetic energy. These coexisting dissociation pathways with same parities but different orbital angular momenta interfere with each other, resulting in the spiral nuclear momentum distribution in the laser polarization plane. The interference structure in the nuclear momentum distribution offers another freedom to identify the dissociation pathways of molecules in strong laser fields.

DOI: 10.1103/PhysRevA.101.033406

With the advent of ultrashort laser technologies, ultrafast physics has attracted attention in past decades [1,2]. Among the fascinating ultrafast phenomena, molecular dissociation is one of the most fundamental processes, and thus has been studied extensively. Because of the simplicity, H_2 and its ion have worked as prototypes for the study of molecular dissociation [3–5] and many dissociation pathways have been explored. The typical dissociation pathways of H_2 are sketched in Fig. 1(a). First of all, one electron of H_2 is stripped off by the laser pulse. Then, the nuclear wave packet of H_2 undergoes the vertical transition (Frank-Condon principle) and starts to relax in the $1s\sigma_g$ potential surface [6]. When the internuclear distance reaches certain values where the energy gap between $1s\sigma_g$ and $2p\sigma_u$ states is close to multiple photon energies, H_2^+ may resonantly absorb several photons if the laser field is still on, and propagate along the $2p\sigma_u$ potential surface. Because of the opposite parities of the $1s\sigma_g$ and $2p\sigma_u$ states, H_2^+ only absorbs odd-number photons, and the most well-known pathways are the one-photon [7] and three-photon [8] dissociation, as sketched by the green and orange arrows respectively. If the laser pulse is long enough, the net-two-photon dissociation [9] (not shown) becomes important. Besides that, dissociation ending with very little energy occurs in single-color pulses via a dynamic Raman process [8] or in two-color laser pulses via absorbing one blue photon and emitting one red photon [10]. Recently, Yamaguchi *et al.* [11] calculated the two-photon dissociation mediated by the excited vibrational state of H_2^+ using the nonuniform optical near field. The different dissociation pathways can be recognized in experiments by calibrating the kinetic-energy releases (KER) of dissociative fragments.

The exploration of different dissociation mechanisms substantially advances the ultrafast physics, particularly, making the molecular dissociation controllable with the ongoing laser technologies. Picón *et al.* [12] realized a many orders-of-magnitude enhancement of the vibrational excitation and dissociation of H_2^+ at infrared wavelengths. Yue *et al.* [13] and Holzmeier *et al.* [14] calculated and confirmed the control of vibration, dissociation, and ionization in intense vacuum ultraviolet laser pulses. The branching ratio of two-photon and three-photon above-threshold dissociation can be controlled by gating the dissociation pathway on a few-femtosecond time scale [15]. The electron localization after the dissociation can be controlled by the carrier-envelope phase of a few-cycle laser pulse [16–24] or the time delay between the attosecond pulse and the infrared pulse [25–27]. Some other strategies of controlling electron localization are also realized, such as two-color laser pulses [28–30], or attosecond pulse train plus the few-cycle laser pulse [31,32]. The electron localization during the dissociation can also be controlled by the ejected electron from H_2 [33,34].

It is generally believed that the one-photon and three-photon dissociation pathways have no energy overlap since the two pathways differ by two photons. However, when H_2^+ stretches to the internuclear distance for one-photon resonant excitation, the nuclear wave packet may already acquire non-negligible kinetic energies [35]. Therefore, after counting on this kinetic energy, the one-photon dissociation pathway might end with the KER which is comparable with the three-photon dissociation pathway. Different from the coexistent one-photon and net-two-photon dissociation pathways with opposite parities, the coexistent one-photon and three-photon pathways have the same parity but different angular momenta, and thus they may interfere with each other.

In this work, we study the dissociation of H_2^+ in a few-cycle circularly polarized laser field with a two-dimensional

*fhe@sjtu.edu.cn

two-channel model. Clear interference structures of one-photon and three-photon dissociation pathways are observed in the nuclear momentum and KER distributions. First, the ground state of H_2 is copied onto the $1s\sigma_g$ state, giving birth to the initial nuclear wave packet depicted by the Franck-Condon approximation. The initial nuclear wave packet isotropically distributes in the polarization plane. After freely propagating the nuclear wave packet for several femtoseconds, a circularly polarized 800-nm laser pulse is then introduced to dissociate the stretched H_2^+. Each cycle of the circularly polarized laser pulse launches the nuclear wave packet from the $1s\sigma_g$ state to the repulsive $2p\sigma_u$ state, creating spiral dissociating nuclear wave packets.

Numerically, we started the simulation just after the single ionization of H_2 by assuming that an isotropic nuclear wave packet of H_2 has been vertically launched onto the $1s\sigma_g$ potential surface by an isolated circularly polarized attosecond pulse. Since the dissociation of H_2^+ mainly relates to the two lowest electronic states, the molecular wave packet of H_2^+ can be approximately written as $\Psi(\mathbf{r},\mathbf{R},t)=\chi_g(\mathbf{R},t)|g\rangle+\chi_u(\mathbf{R},t)|u\rangle$, where $|g\rangle$ and $|u\rangle$ are the $\mathbf{R}$-parametric electron wave functions in the $1s\sigma_g$ and $2p\sigma_u$ states, respectively [36]. $\mathbf{r}$ and $\mathbf{R}$ denote the electron displacement and the internuclear displacement. $\chi_g(\mathbf{R},t)$ and $\chi_u(\mathbf{R},t)$ are the nuclear wave packets associated with $|g\rangle$ and $|u\rangle$. In our simulations, $\mathbf{R}$ is restricted in the two-dimensional laser polarization plane (R_x, R_y). The dissociation of H_2^+ is governed by the two-channel time-dependent Schrödinger equation (TDSE) [36] (atomic units are used throughout unless otherwise stated),

$$i\frac{\partial}{\partial t}\begin{pmatrix}\chi_g(R_x,R_y,t)\\ \chi_u(R_x,R_y,t)\end{pmatrix}=(H_0+H_I)\begin{pmatrix}\chi_g(R_x,R_y,t)\\ \chi_u(R_x,R_y,t)\end{pmatrix} \quad (1)$$

with

$$H_0=\begin{pmatrix}\frac{P_x^2+P_y^2}{2M}+V_g(R_x,R_y) & 0\\ 0 & \frac{P_x^2+P_y^2}{2M}+V_u(R_x,R_y)\end{pmatrix} \quad (2)$$

and

$$H_I=\begin{pmatrix}0 & D(R_x,R_y)F(t)\\ D(R_x,R_y)F(t) & 0\end{pmatrix}, \quad (3)$$

where $M=918$ a.u. is the reduced nuclear mass, P_x and P_y are the nuclear momentum operators, and $V_g(R_x,R_y)$ and $V_u(R_x,R_y)$ are the potential surfaces for the $1s\sigma_g$ and $2p\sigma_u$ states, respectively. $F(t)$ is the laser field to be used. $D(R_x,R_y)$ is the dipole matrix representing the coupling between the two electronic states. At the beginning of the simulation, $\chi_g(R_x,R_y,t=0)$ is set to be the ground nuclear wave packet of H_2, which is obtained by imaginarily propagating a guessed function on the $X^1\Sigma_g^+$ potential surface of H_2 until the energy fluctuation is less than 10^{-15} [37]. No population is on the $2p\sigma_u$ state initially, i.e., $\chi_u(R_x,R_y,t=0)=0$. After the laser-H_2^+ interaction, we kept propagating the nuclear wave packet until the dissociative part clearly separates from the bound vibrational states. By Fourier transforming the dissociative wave packet, we obtained the nuclear momentum wave packet, from which the energy distribution can be further achieved. We used the split-operator algorithm to propagate the wave packets [38]. The spatial steps are $dR_x=dR_y=0.04$ a.u., and the time step is $dt=0.2$ a.u. The simulation box is big enough to hold all wave packets during the interaction and thereby no absorbing boundaries are needed.

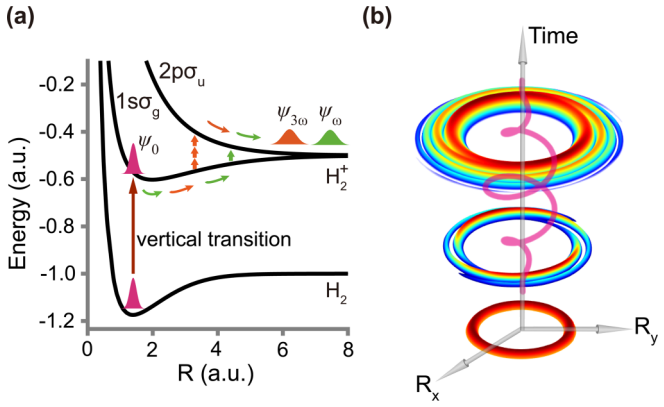

FIG. 1. (a) The related potential curves for the ultrafast reaction of H_2 in strong laser fields and the sketch of one-photon and three-photon dissociation of H_2^+. (b) The time evolution of dissociated nuclear wave packets of Franck-Condon state H_2^+ in a few-cycle circularly polarized laser pulse. Clear spiral structures finally come into being in the wave packets.

After freely propagating the initial nuclear wave packet on the $1s\sigma_g$ surface for $\Delta t=5$ fs, we introduced the laser field

$$\mathbf{F}(t)=E_0\{\cos[\omega(t-\Delta t)+\alpha]\hat{x}+\sin[\omega(t-\Delta t)+\alpha]\hat{y}\}\times\sin^2[\pi(t-\Delta t)/\tau],\quad \Delta t<t<\tau+\Delta t \quad (4)$$

to dissociate H_2^+ to different directions. α is the carrier envelope phase. The laser intensity is $10^{14}\,\mathrm{W/cm^2}$, $\tau=4T$ with the optical cycle $T=2\pi/\omega$ and $\omega=0.057$ a.u. We depict the time evolution of dissociated nuclear wave packets in Fig. 1(b). Also the movies for nuclear wave packet propagation with and without the circularly polarized field applied can be found in the Supplemental Material [39]. Figures 2(a) and 2(b) show the momentum distributions of nuclei dissociated along the $1s\sigma_g$ and $2p\sigma_u$ potential surfaces. One may clearly see spiral structures in nuclear momentum distributions, which share a similar structure observed in photoionization [40–43]. The spiral nuclear momentum distribution can be transformed into the angle-resolved KER distribution, as shown in Figs. 2(c) and 2(d).

As shown in Figs. 2(a) and 2(b), the dissociation along the $2p\sigma_u$ state has the dominant probability over the dissociation along the $1s\sigma_g$ state for the laser parameters used, thus we first focus on the dissociation along the $2p\sigma_u$ state. The angle-resolved KER distribution shown in Fig. 2(d) can be roughly grouped into two parts. The part with a dominating probability in the energy range below 1.2 eV presents an almost horizontal band. The high-energy part (>1.2 eV), which has a much smaller probability, presents several stripes with the energy separation about 0.5 eV. The low-energy part is recognized as the one-photon dissociation by resonantly absorbing one photon at $R=4.74$ a.u., which has been discussed extensively [7,24]. The stripes covering the energy range from 1.2 to 3 eV have never been observed before as far as we know.

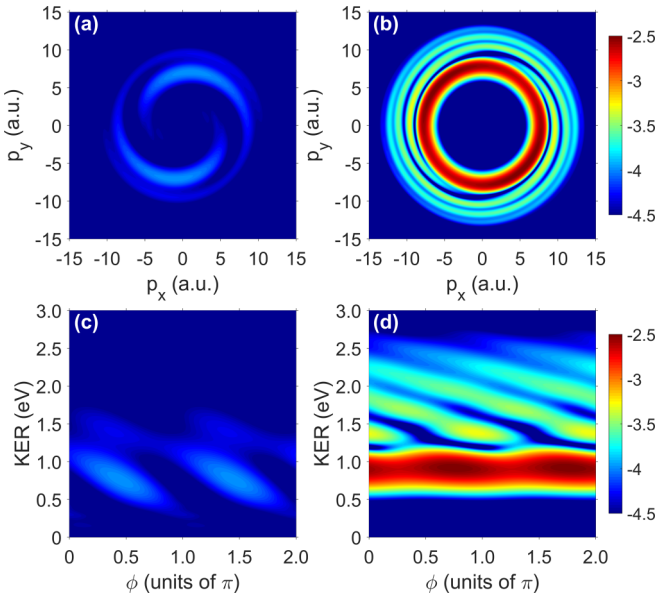

FIG. 2. (a),(b) The momentum distributions contributed by the dissociation along the $1s\sigma_g$ state and $2p\sigma_u$ state respectively. (c),(d) The angle-resolved KER distributions contributed by the dissociation along the $1s\sigma_g$ state and $2p\sigma_u$ state respectively. The laser central wavelength, pulse duration and intensity are 800 nm, $4T$, and 10^{14} W/cm^2.

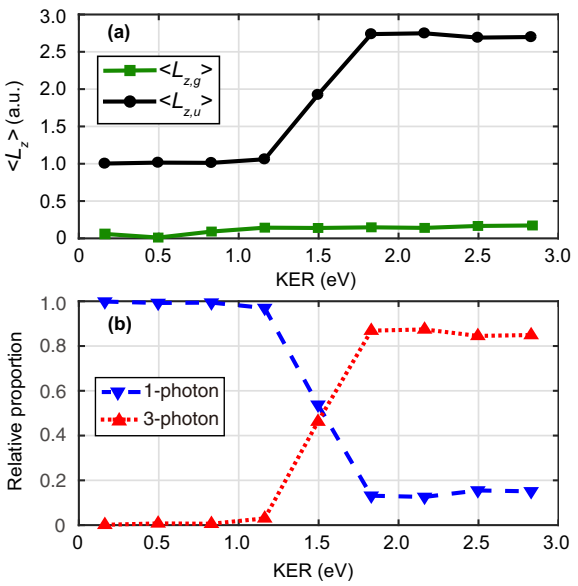

FIG. 3. (a) The KER-dependent angular momenta contributed by the dissociation along the $1s\sigma_g$ state (the green line with squares) and $2p\sigma_u$ state (the black line with circles). (b) The KER-dependent relative proportions of one-photon pathway (the blue line with lower triangles) and three-photon pathway (the red line with upper triangles). The laser parameters are the same as those used in Fig. 2.

Since all these dissociative fragments shown in Fig. 2(d) are purely contributed by the dissociation along the $2p\sigma_u$ state, the dissociation must be induced by absorbing odd numbers of photons according to the parity conservation [24]. Due to the broad initial nuclear kinetic-energy distribution acquired during the molecular stretching, the KER obtained by absorbing different photons may overlap each other, which impedes to identify the absorbed photon numbers in the energy spectra. However, according to the angular momentum conservation in the interaction, the angular momenta of the dissociative fragments directly map the absorbed photon numbers since the angular momentum of H_2^+ is absolutely zero just after the single ionization of H_2. The expected KER-dependent angular momentum along the laser propagation direction for the fragments dissociated along the $2p\sigma_u$ potential surface is $\langle L_{z,u}(\mathrm{KER})\rangle = \langle\tilde{\chi}_u(\mathrm{KER},\phi)|\mathbf{R}\times\mathbf{P_R}|\tilde{\chi}_u(\mathrm{KER},\phi)\rangle$, where ϕ is the nuclear emission angle. The angle-resolved nuclear energy wave packet $\tilde{\chi}_u(\mathrm{KER},\phi)$ is transformed from the final dissociative nuclear wave packet in momentum representation. Similarly, the angular momentum $\langle L_{z,g}(\mathrm{KER})\rangle$ for the dissociation along the $1s\sigma_g$ state can also be calculated by $\langle L_{z,g}(\mathrm{KER})\rangle = \langle\tilde{\chi}_g(\mathrm{KER},\phi)|\mathbf{R}\times\mathbf{P_R}|\tilde{\chi}_g(\mathrm{KER},\phi)\rangle$. Specifically, we equally divided the nuclear wave packets of Fig. 2(c) [or 2(d)] into nine parts for different KER ranges with the sampling interval $\Delta\mathrm{KER} = 0.33$ eV, and then the expected angular momentum $\langle L_{z,g}(\mathrm{KER})\rangle$ [or $\langle L_{z,u}(\mathrm{KER})\rangle$] of every part can be obtained. The results are shown in Fig. 3(a). For the dissociation along $2p\sigma_u$ potential surface, the angular momentum is exactly 1 for the events having energy less than 1 eV, which indicates that H_2^+ absorbs one photon and undergoes the pure one-photon dissociation pathway. For the KER in the range of [1.2 eV, 3 eV], the expected angular momentum varies between 1 and 3, which indicates the mixture of the one-photon and three-photon dissociation pathways if events of absorbing five or even more photons are negligible. For the dissociation along the $1s\sigma_g$ potential surface, the angular momentum is very close to zero, which suggests that the zero-photon process is the main dissociation pathway and net-two-photon dissociation contributes a little. Thus, the stripes in Fig. 2(c) are induced by the interference of zero-photon and net-two-photon dissociation pathways.

With the expected angular momenta, one may formulate the proportions of zero-, two-, one-, and three-photon pathways as $W_0(\mathrm{KER}) = 1 - \langle L_{z,g}(\mathrm{KER})\rangle/2$, $W_2(\mathrm{KER}) = \langle L_{z,g}(\mathrm{KER})\rangle/2$, $W_1(\mathrm{KER}) = [3 - \langle L_{z,u}(\mathrm{KER})\rangle]/2$, and $W_3(\mathrm{KER}) = [\langle L_{z,u}(\mathrm{KER}) - 1\rangle]/2$. Figure 3(b) shows the relative proportion when H_2^+ dissociates along the $2p\sigma_u$ potential surface.

As a verification of the above conclusion based on the angular momentum analysis, we reproduced the interference of different dissociation pathways with a perturbation analysis. Specifically, we expanded the nuclear wave packet perturbatively in the Lippmann-Schwinger equation [44], i.e.,

$$\chi(R_x,R_y,t) = \chi_0(R_x,R_y,t) + \chi_1(R_x,R_y,t) + \chi_2(R_x,R_y,t) + \chi_3(R_x,R_y,t) + \cdots, \quad (5)$$

where

$$\chi_n(R_x,R_y,t) = \begin{pmatrix}\chi_{gn}(R_x,R_y,t)\\ \chi_{un}(R_x,R_y,t)\end{pmatrix}$$

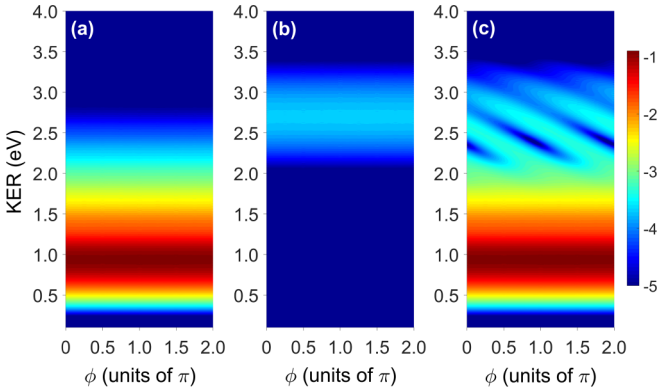

FIG. 4. The interference of different pathways carrying different angular momenta from perturbation theory. (a) The angle-resolved KER distribution of one-photon pathway. (b) The angle-resolved KER distribution of three-photon pathway. (c) The coherent addition of (a) and (b). The laser parameters are the same as those used in Fig. 2.

represents the wave packet of absorbing n photons, and

$$\chi_0(R_x, R_y, t) = e^{-iH_0(t-t_0)}\chi_0(R_x, R_y, t_0), \tag{6}$$

$$\chi_1(R_x, R_y, t) = -i\int_{t_0}^{t} dt_1 e^{-iH_0(t-t_1)}H_1(t_1)\chi_0(R_x, R_y, t_1), \tag{7}$$

$$\chi_2(R_x, R_y, t) = -i\int_{t_0}^{t} dt_2 e^{-iH_0(t-t_2)}H_1(t_2)\chi_1(R_x, R_y, t_2), \tag{8}$$

$$\chi_3(R_x, R_y, t) = -i\int_{t_0}^{t} dt_3 e^{-iH_0(t-t_3)}H_1(t_3)\chi_2(R_x, R_y, t_3). \tag{9}$$

Here, $\chi_2(R_x, R_y, t)$ is a virtual state of absorbing two photons, which is mediated to the three-photon pathway. Since the pulse used in this research is short and not very strong, for exploring mechanisms, we only concern the two most relevant photon absorption channels here, namely the one-photon and three-photon pathways, which mainly contribute to the interference fringes of the TDSE result in Fig. 2(d). The Rabi flopping between $1s\sigma_g$ and $2p\sigma_u$ states cannot be reproduced in this perturbation calculation. Once having $\chi_1(R_x, R_y, t)$ and $\chi_3(R_x, R_y, t)$ after the interaction, we are able to plot the angle-resolved KER distributions for one-photon and three-photon pathways, as shown in Figs. 4(a) and 4(b). The coherent addition of Figs. 4(a) and 4(b), shown in Fig. 4(c), presents the interference stripes. The difference of Figs. 4(c) and 2(d) might be due to the truncation of higher-order perturbation and the missing photon emission. Nevertheless, the approximated perturbation calculations already reconstruct the interference stripes qualitatively.

After identifying the dissociation pathways, we are ready to analyze how the interference stripes in Fig. 2 are formed. Approximately, the wave function of one-photon and three-photon dissociated nuclear wave packets can be expressed as $A_1(E)e^{i(\phi+\alpha)}$ and $A_3(E)e^{i[3(\phi+\alpha)+\eta_u(\mathrm{KER})]}$ respectively [42], where $\eta_u(\mathrm{KER})$ is a \textrmKER-dependent phase difference between the two dissociation pathways. $A_1(\mathrm{KER})$ and $A_3(\mathrm{KER})$ are the amplitudes of them. Then the interference given by one- and three-photon dissociation pathways can be formulated as

$$S_u(\phi, \mathrm{KER}) = A_1^2(\mathrm{KER}) + A_3^2(\mathrm{KER}) + 2A_1(\mathrm{KER})A_3(\mathrm{KER}) \times \cos[2(\phi+\alpha) + \eta_u(\mathrm{KER})]. \tag{10}$$

Similarly, the interference of the zero-photon and net-two-photon pathways can be formulated as

$$S_g(\phi, \mathrm{KER}) = A_0^2(\mathrm{KER}) + A_2^2(\mathrm{KER}) + 2A_0(\mathrm{KER})A_2(\mathrm{KER}) \times \cos[2(\phi+\alpha) + \eta_g(\mathrm{KER})], \tag{11}$$

where $A_0(\mathrm{KER})$, $A_2(\mathrm{KER})$, and $\eta_g(\mathrm{KER})$ are the amplitudes and KER-dependent phase difference of the two dissociation pathways. As shown in Figs. 2(c) and 2(d), the period for the horizontal interference pattern is π, which is decided by the π periodicity of the dependence of S_g and S_u on ϕ respectively. We have also tested that the interference stripes in Figs. 2(c) and 2(d) shift horizontally if the carrier-envelope phase α of the driving laser field changes. The shift of π of α gives the identical angle-resolved KER distribution. The vertical interference patterns in Figs. 2(c) and 2(d) are determined by $\eta_g(\mathrm{KER})$ and $\eta_u(\mathrm{KER})$ respectively, which are accumulated during the molecular bond stretching on the potential surfaces and may help to resolve the nuclear motion. For instance, $\eta_u(\mathrm{KER})$ could be extracted from Fig. 2(d), by which one can evaluate the time delay of one- and three-photon dissociation pathways, similar to the discussions in ionization researches [43].

The spiral interference fringes in the nuclear wave packets given by our two-channel model are reliable. Owing to the few-cycle pulse used in this work, the internuclear distance is small during the laser-H_2^+ interaction, and thus the charge-resonance-enhanced ionization can be ignored. The coupling between the two lowest electronic states is much stronger than others, so contributions from high electronic states are negligible. The features shown in Fig. 2 are robust to the laser intensity, which has been verified by changing the laser intensity around one order of magnitude. Therefore one may observe the spiral interference fringes in experiment with the current laser technology soon afterwards. The interference fringes in our nuclear probability distributions are induced by the mixture of two pathways with the same parity, while the asymmetry of electron localization [19,21,24] is produced by the interference of two pathways with the different nuclear parities, and thus they are clearly different.

In conclusion, the broad kinetic-energy distribution acquired in the molecular bond free stretching offers distinguished initial velocities for H_2^+ to undergo one-photon and three-photon dissociation, thus the two dissociative pathways may end with the same ultimate kinetic energy, and then they interfere with each other. The interference of superimposed pathways carrying different angular momenta contributes to the spiral nuclear momentum distribution and striped angle-resolved kinetic distributions. The interference of different pathways carrying different orbital angular momenta is general, and can be realized by conceiving different experiments. For example, the counter-rotating two-color laser pulse may trigger the nuclear wave packets with the orbital angular

momenta $-\hbar$ and $\hbar$ and thus bring the $\cos(2\phi)$ interference stripes. With a longer wavelength, the one-photon and five-photon dissociation pathways may have overlapped energy, which may bring the $\cos(4\phi)$ interference structure. Our study shows that one may extract the information of the initial nuclear kinetic-energy distribution of H_2^+ before photon absorption. The phase information encoded in the interference fringes is helpful to obtain additional information about the movements of nuclei, e.g., the time delay of two dissociative channels.

ACKNOWLEDGMENTS

This work was supported by National Key R&D Program of China (Grant No. 2018YFA0404802), Innovation Program of Shanghai Municipal Education Commission (Grant No. 2017-01-07-00-02-E00034), National Natural Science Foundation of China (NSFC) (Grants No. 11925405, No. 11721091, and No. 91850203), and Shanghai Shuguang Project (17SG10). Simulations were performed on the π supercomputer at Shanghai Jiao Tong University.

[1] F. Krausz and M. Ivanov, Rev. Mod. Phys. **81**, 163 (2009).

[2] M. Nisoli, P. Decleva, F. Calegari, A. Palacios, and F. Martín, Chem. Rev. **117**, 10760 (2017).

[3] C. R. Calvert, W. A. Bryan, W. R. Newell, and I. D. Williams, Phys. Rep. **491**, 1 (2010).

[4] H. Ibrahim, C. Lefebvre, A. D. Bandrauk, A. Staudte, and F. Légaré, J. Phys. B **51**, 042002 (2018).

[5] H. Li, X. C. Gong, K. Lin, R. D. V. Riedle, X. M. Tong, J. Wu, and M. F. Kling, J. Phys. B **50**, 172001 (2017).

[6] H. Niikura, D. M. Villeneuve, and P. B. Corkum, Phys. Rev. A **73**, 021402(R) (2006).

[7] P. H. Bucksbaum, A. Zavriyev, H. G. Muller, and D. W. Schumacher, Phys. Rev. Lett. **64**, 1883 (1990).

[8] A. Giusti-Suzor and F. H. Mies, Phys. Rev. Lett. **68**, 3869 (1992).

[9] A. Staudte, D. Pavičić, S. Chelkowski, D. Zeidler, M. Meckel, H. Niikura, M. Schöffler, S. Schössler, B. Ulrich, P. P. Rajeev, T. Weber, T. Jahnke, D. M. Villeneuve, A. D. Bandrauk, C. L. Cocke, P. B. Corkum, and R. Dörner, Phys. Rev. Lett. **98**, 073003 (2007).

[10] X. H. Xie, S. Roither, S. Larimian, S. Erattupuzha, L. Zhang, D. Kartashov, F. He, A. Baltuška, and M. Kitzler, Phys. Rev. A **99**, 043409 (2019).

[11] M. Yamaguchi and K. Nobusada, Phys. Rev. A **93**, 023416 (2016).

[12] A. Picón, A. Jaron-Becker, and A. Becker, Phys. Rev. Lett. **109**, 163002 (2012).

[13] L. Yue and L. B. Madsen, Phys. Rev. Lett. **115**, 033001 (2015).

[14] F. Holzmeier, R. Y. Bello, M. Hervé, A. Achner, T. M. Baumann, M. Meyer, P. Finetti, M. DiFraia, D. Gauthier, E. Roussel, O. Plekan, R. Richter, K. C. Prince, C. Callegari, H. Bachau, A. Palacios, F. Martín, and D. Dowek, Phys. Rev. Lett. **121**, 103002 (2018).

[15] J. McKenna, F. Anis, A. M. Sayler, B. Gaire, N. G. Johnson, E. Parke, K. D. Carnes, B. D. Esry, and I. Ben-Itzhak, Phys. Rev. A **85**, 023405 (2012).

[16] M. F. Kling, C. Siedschlag, A. J. Verhoef, J. I. Khan, M. Schultze, T. Uphues, Y. Ni, M. Uiberacker, M. Drescher, F. Krausz, and M. J. J. Vrakking, Science **312**, 246 (2006).

[17] V. Roudnev, B. D. Esry, and I. Ben-Itzhak, Phys. Rev. Lett. **93**, 163601 (2004).

[18] V. Roudnev and B. D. Esry, Phys. Rev. Lett. **99**, 220406 (2007).

[19] M. Kremer, B. Fischer, B. Feuerstein, V. L. B. de Jesus, V. Sharma, C. Hofrichter, A. Rudenko, U. Thumm, C. D. Schröter, R. Moshammer, and J. Ullrich, Phys. Rev. Lett. **103**, 213003 (2009).

[20] B. Fischer, M. Kremer, T. Pfeifer, B. Feuerstein, V. Sharma, U. Thumm, C. D. Schröter, R. Moshammer, and J. Ullrich, Phys. Rev. Lett. **105**, 223001 (2010).

[21] I. Znakovskaya, P. von den Hoff, G. Marcus, S. Zherebtsov, B. Bergues, X. Gu, Y. Deng, M. J. J. Vrakking, R. Kienberger, F. Krausz, R. de Vivie-Riedle, and M. F. Kling, Phys. Rev. Lett. **108**, 063002 (2012).

[22] F. Anis and B. D. Esry, Phys. Rev. Lett. **109**, 133001 (2012).

[23] T. Rathje, A. M. Sayler, S. Zeng, P. Wustelt, H. Figger, B. D. Esry, and G. G. Paulus, Phys. Rev. Lett. **111**, 093002 (2013).

[24] N. G. Kling, K. J. Betsch, M. Zohrabi, S. Zeng, F. Anis, U. Ablikim, B. Jochim, Z. Wang, M. Kübel, M. F. Kling, K. D. Carnes, B. D. Esry, and I. Ben-Itzhak, Phys. Rev. Lett. **111**, 163004 (2013).

[25] F. He, C. Ruiz, and A. Becker, Phys. Rev. Lett. **99**, 083002 (2007).

[26] F. Kelkensberg, C. Lefebvre, W. Siu, O. Ghafur, T. T. Nguyen-Dang, O. Atabek, A. Keller, V. Serov, P. Johnsson, M. Swoboda, T. Remetter, A. L'Huillier, S. Zherebtsov, G. Sansone, E. Benedetti, F. Ferrari, M. Nisoli, F. Lépine, M. F. Kling, and M. J. J. Vrakking, Phys. Rev. Lett. **103**, 123005 (2009).

[27] G. Sansone, F. Kelkensberg, J. F. P. Torres, F. Morales, M. F. Kling, W. Siu, O. Ghafur, P. Johnsson, M. Swoboda, E. Benedetti, F. Ferrari, F. Lépine, J. L. S. Vicario, S. Zherebtsov, I. Znakovskaya, A. L'Huillier, M. Y. Ivanov, M. Nisoli, F. Martín, and M. J. J. Vrakking, Nature (London) **465**, 763 (2010).

[28] D. Ray, F. He, S. De, W. Cao, H. Mashiko, P. Ranitovic, K. P. Singh, I. Znakovskaya, U. Thumm, G. G. Paulus, M. F. Kling, I. V. Litvinyuk, and C. L. Cocke, Phys. Rev. Lett. **103**, 223201 (2009).

[29] X. Gong, P. He, Q. Song, Q. Ji, H. Pan, J. Ding, F. He, H. Zeng, and J. Wu, Phys. Rev. Lett. **113**, 203001 (2014).

[30] H. Xu, Z. C. Li, F. He, X. Wang, A. A. T. Noor, D. Kielpinski, R. T. Sang, and I. V. Litvinyuk, Nat. Commun. **8**, 15849 (2017).

[31] K. P. Singh, F. He, P. Ranitovic, W. Cao, S. De, D. Ray, S. Chen, U. Thumm, A. Becker, M. M. Murnane, H. C. Kapteyn, I. V. Litvinyuk, and C. L. Cocke, Phys. Rev. Lett. **104**, 023001 (2010).

[32] F. He and U. Thumm, Phys. Rev. A **81**, 053413 (2010).

[33] M. Waitz, D. Aslitürk, N. Wechselberger, H. K. Gill, J. Rist, F. Wiegandt, C. Goihl, G. Kastirke, M. Weller, T. Bauer, D. Metz, F. P. Sturm, J. Voigtsberger, S. Zeller, F. Trinter, G. Schiwietz, T. Weber, J. B. Williams, M. S. Schöffler, L. P. H. Schmidt, T. Jahnke, and R. Dörner, Phys. Rev. Lett. **116**, 043001 (2016).

[34] V. V. Serov and A. S. Kheifets, Phys. Rev. A **89**, 031402(R) (2014).

[35] J. Zhang, G. Q. He, and F. He, Mol. Phys. **112**, 1929 (2014).
[36] E. Charron, A. G. Suzor, and F. H. Mies, J. Chem. Phys. **103**, 7359 (1995).
[37] R. Kosloff and H. T. Ezer, Chem. Phys. Lett. **127**, 223 (1986).
[38] R. Kosloff and D. Kosloff, J. Comput. Phys. **52**, 35 (1983).
[39] See Supplemental Material at http://link.aps.org/supplemental/10.1103/PhysRevA.101.033406 for animations: The first animation, S1, shows the free evolution of the Franck-Condon state H_2^+ wave function on the potential curve of the $1s\sigma_g$ state (nuclear revival movement). The second animation, S2, shows the time evolution of dissociative state nuclear wave packets when a circularly polarized few-cycle field is applied. The laser parameters are the same as those used in Fig. 2.
[40] J. M. Ngoko Djiokap, S. X. Hu, L. B. Madsen, N. L. Manakov, A. V. Meremianin, and A. F. Starace, Phys. Rev. Lett. **115**, 113004 (2015).
[41] J. M. Ngoko Djiokap, A. V. Meremianin, N. L. Manakov, S. X. Hu, L. B. Madsen, and A. F. Starace, Phys. Rev. A **94**, 013408 (2016).
[42] D. Pengel, S. Kerbstadt, D. Johannmeyer, L. Englert, T. Bayer, and M. Wollenhaupt, Phys. Rev. Lett. **118**, 053003 (2017).
[43] D. Pengel, S. Kerbstadt, L. Englert, T. Bayer, and M. Wollenhaupt, Phys. Rev. A **96**, 043426 (2017).
[44] B. A. Lippmann and J. Schwinger, Phys. Rev. **79**, 469 (1950).